STScI | SPACE TELESCOPE SCIENCE INSTITUTE

Instrument Science Report WFC3 2021-15

WFC3/UVIS Tungsten Lamp and Filter Performance 2009-2021

Harish Khandrika, Benjamin Kuhn

September 21, 2021

Abstract

We examine Wide Field Camera 3 UVIS internal flat-field images acquired with the tungsten lamp#3 to check for any changes in the filters over time as well as report on the performance of the lamp. The data for this study were acquired from Cycle 17 through Cycle 28 (May 2009-March 2021). UVIS flat-field images show an overall decrease in countrates from 1-4% over the last 12 years depending on wavelength. Bluer wide-band filters show greater loss in performance compared to redder filters, indicating a possible reddening of the lamp over time. This decrease in brightness is principally associated with the photometric sensitivity losses observed by previous reports as the level of sensitivity loss matches the tungsten flat image ratio levels. Several new artifacts of unknown origin have been noted in the filter ratio images, most notably a dark patchy region in amps A and B for the bluer filters. There is also a rectangular-shaped dark region (on multiple filters in amp B), whose right edge coincides with one of the lithography mask lines. Both the patch and the rectangular area regions show a decrease in brightness larger than the median value of the filter ratio and typically on the order of 2-5%. No new dust motes or droplets have been discovered since SMOV in 2009 and the existing particulates have shown that, as noted in prior studies (e.g. Bourque and Baggett 2013), some filter wheels occasionally do not return to precisely the same position. This offset does not impact external science observations. Lastly, we note that the flat-fields shown here are completely internal and are not used in the pipeline processing for flat-field correction.

1 Introduction

To aid in monitoring the performance of the UVIS detector, the Wide Field Camera 3 (WFC3) instrument has four tungsten lamps (and one deuterium lamp) that are used to obtain internal flat-field images (flats). Any of the four tungsten bulbs can physically be used with either the UVIS or IR detector, but for routine on-orbit observations only lamp 3 is used with UVIS. A single tungsten lamp illuminates the detector for a period of time and the resulting image is used to monitor the pixel-to-pixel variations in the detectors, filter performance, and other effects. The lamps all reside in a separate calibration subsystem which has a significantly different f ratio from the external beam (f/300 instead of f/31; Baggett, Sabbi, and McCullough 2009). Because of this, the internal flat-fields will show features that are not normally seen in external science images. Furthermore, the internal flat-fields are used for monitoring purposes only and not for calibration pipeline flat-fields. Previous studies of the UVIS flat-field images have focused on improving photometric performance with new flat-field reference files (Mack, Sabbi, and Dahlen 2013), observing tungsten lamp performance using the bowtie monitor (Bourque and Baggett 2013), and looking at changes in pixel-to-pixel flat fields (Gunning, Baggett, and MacKenty 2014). In this report we analyze nearly 12 years of internal flat-field images obtained via the tungsten lamp since the Servicing Mission Observatory Verification (SMOV) in May 2009 when WFC3 was installed. This report extends the understanding and analysis of the previous work and aims to characterize the overall performance and possible degradation of the tungsten lamp.

2 Data and Methods

Data were obtained through the MAST Hubble Archive and consisted of full-frame unbinned tungsten lamp images with no charge injection. The tungsten lamp observations from the Extended Pixel Edge Response calibration program (for all years) were excluded due to their unique observation format that creates larger overscan areas. The resulting sets of data comprised 8540 images taken in 34 filters via 58 proposals/programs spanning from May 29 2009 until March 06 2021. A full list of all programs, filters, dates, and number of images can be seen in Table 1. Images used in the analysis consisted of calibrated data (FLT) [using the calwf3 pipeline v 3.5.3] as well as CTE-corrected calibrated data (FLC). FLC data were checked primarily to verify that any artifacts or supposed changes in lamp sensitivity were not due directly to charge transfer inefficiencies. All flat-field images were taken using tungsten lamp 3.

Tungsten images were analyzed on a filter-by-filter basis. In order to search for any changes in lamp brightness over time, we compared data within a filter between an observed time period to SMOV. In our analysis, SMOV data (program 11432) were treated as unity or reference, given that it was the first set of data taken after WFC3 installation into HST in May 2009. Lamp brightness was checked by comparing FLT to SMOV count-rates (counts/s) since data taken for a particular filter may have different exposure times leading to different count levels. The median ratio between FLT and SMOV count-rates for each chip was then tracked over time per filter.

In addition to checking overall lamp performance per filter, more careful visual inspections

for new artifacts or changes were performed by comparing individual images taken each year to SMOV. We looked for the presence of new artifacts such as new dust motes or bubbles as well as any large-scale changes in the flats themselves.

3 Analysis

3.1 Overall Lamp Performance Over Time

Figure 1 shows the ratio between the 2021 (or latest) tungsten lamp data (FLT) versus SMOV data for each filter, represented by the filter's pivot wavelength. For the majority of filters, there is an overall drop in lamp performance of 1-4% from SMOV to 2021, the exact values for each filter are shown in Table 3. We confirmed the changes in the lamp performance were not due to Charge Transfer Inefficiency (CTI) by evaluating results on both FLC and FLT data, as also shown in Figure 1. With this indication that CTI is not the main cause, we complete the rest of the analysis on FLT data directly. Figure 1 also overplots the photometric sensitivity loss of the UVIS detector between 2009 and 2021 as computed by Calamida et al. (2021). As seen in the figure, the ratio of tungsten internal flat-field images in filters with a pivot wavelength larger than 4500 Å show similar performance characteristics to the photometry, indicating that overall the apparent changes in the tungsten lamp flux are attributable to photometric sensitivity loss. For filters with a pivot wavelength smaller than or equal to 4500 Å we note that the ratio does drop below the photometric sensitivity loss for those bandwidths. The tungsten bulb's filament temperature is 2700 K (ISR 2009-28) and as such, its output flux at bluer wavelengths is considerably lower than at redder wavelength so the error bars on our measurements could be larger. Furthermore, the filament may be cooling over time which would shift its blackbody output to the red. F336W and F343N data were only available from 2009 to 2010 and 2011 (respectively), while all other filters were characterized over the entire period, 2009 to 2021. Figures showing the ratios to SMOV for every filter across all 10-11 years and ratio images for all years are available on the UVIS calibration subsystem webpage (https://www.stsci.edu/hst/instrumentation/wfc3/performance/cal-subsystem). Table 4 summarizes the prominent features for several filters as noted by the flat-field ratio images.

3.2 New Image Artifacts in Tungsten Internal Flat-Fields

3.2.1 The Bowling Pin

A region of the internal flat-field ratio images in some low bandwidth filters between amps A and B appear darker, that is, the pixels exhibit a lower ratio level compared to the rest of the flat image. This was first noted in F390W from the 2014 ratio image onwards but can be seen in filters F410M, F438W, F467M, F469N, and F475W. This is hereafter referred to as the Bowling Pin and Figure 2 shows an example of this in the F390W 2020 image ratio. Analysis of the F390W 2020 ratio shows that the count-rate level in the Bowling Pin is up to 5% less than the levels in SMOV. As the filter bandpass shifts into the visible wavelengths,

from F390W to F475W, the Bowling Pin seems to match the ratio of the rest of the flat-field image, disappearing entirely by F547M. The cause for this feature remains unknown at this time. It does not appear related to the UVIS flare effect (Mack, Sabbi, and Dahlen (2013)): the shape of the flare extends towards the second chip and does not entirely match the shape of the Bowling Pin, as shown in Figure 3. The overall flare shape has also not changed between the 2020 image and the 2009 SMOV image, and only a slight darkening (decrease in ratio) between one image and another can be seen. We examined dark images between 2012/2013 and 2021 with a high post-flash level (in order to let the darker patch stand out). Figure 4 shows the ratio of darks with a post-flash level of 7310 electrons/pixel, and the image reveals no patchiness or significant feature. Thus the Bowling Pin is likely not an issue within the CCD although that cannot be completely ruled out: the LED which generates the post-flash is quite red ($>$ 8000 Å) and the dark AB patch is not seen in any internal flat-fields redder than $\sim$ 5000 Å.

3.2.2 Roller Shade

A region of the flat-field ratio images in the F390W, F438W, F657N, and F658N filters contains a rectangular section on the amp B side close to the chip gap with a lower image ratio value than the rest of the image, which we've dubbed the "Roller Shade". Figure 6 shows an example of this in F658N for 2020 compared to SMOV. For the 2020 ratio image, the region corresponds to a 2.5-3.5% drop in flux between 2009 and 2020. From 2011 on this region drops in flux year-by-year, being less visible in 2011 and more apparent in the more recent images. The roller shade appeared $\sim$2011 and seems to have deepened over time. Figures 7 and 9 show the roller shade effect in F438W and F657N respectively. In F390W, the effect is 1% dimmer than the rest of the flat-field by 2020, in F438W, the effect is 2% dimmer by 2021 and in F657N the effect is less than 1% dimmer. The lithographic mask pattern (an artifact from the CCD manufacturing process) results in a large-scale (6x2) grid pattern across each chip. This pattern can be seen in the astrometric data analyses [Kozhurina-Platais et al. (2013), see Fig 4]. Although the cause of the roller shade region is unknown, we note that right edge of the roller shade coincides with one of these lithographic lines.

3.3 Known Image Artifacts in Tungsten Internal Flat-Fields

3.3.1 Bright regions

F645N flat-field images exhibit an interesting H-shaped patterned region encompassing amp A and amp B, first noted in Baggett, Sabbi, and McCullough (2009). An example image ratio can be seen in Figure 8 for 2021. Bright regions in F657N are also noted by Baggett, Sabbi, and McCullough (2009) present in amps B and D and can be seen as darker regions in Figure 9. The ratios of these regions compared to SMOV seem to be less than the overall median ratio for the entire flat by 1-2% on average.

A group of pixels in the lower left corner of the F410M flat-field ratio images exhibits an unusual structure. This structure can be seen in the flat-field images from SMOV onward, changing slightly in shape from 2010 to 2011 in the ratio images, and remaining mostly the

same from 2011 to 2021. Figure 5 shows the F410M defect in 2010 and 2021. The majority of the region is brighter by about 2-4% between the 2021 image and the 2009 image, indicating a possible change to the filter. This defect has been noted by Rajan and Baggett (2010). During thermal-vacuum (TV) testing on the ground Baggett (2008) reported seeing scattered light from beveled filter edges in F410M, which could be the reason for the defect.

3.3.2 Dust motes and droplets

Baggett, Sabbi, and McCullough (2009) notes the presence of "droplets" caused by mineral condensation residue on the flat-field images as well as the presence of dust motes. We combed through every tungsten image for all filters through all years and found no new droplets or dust motes on any images. Figure 7 shows very clear dust motes (and droplets) in the ratio image for F438W for 2014. The dust motes are not always visible in every ratio image for F438W (or other filters). The shifts in position of the dust motes are consistent with the filter wheel not returning to the same position and being offset by 0.5 deg or 1 wheel step (Bourque and Baggett (2013)). Droplets also seem shifted slightly in most images, indicating a potential filter shift after SMOV.

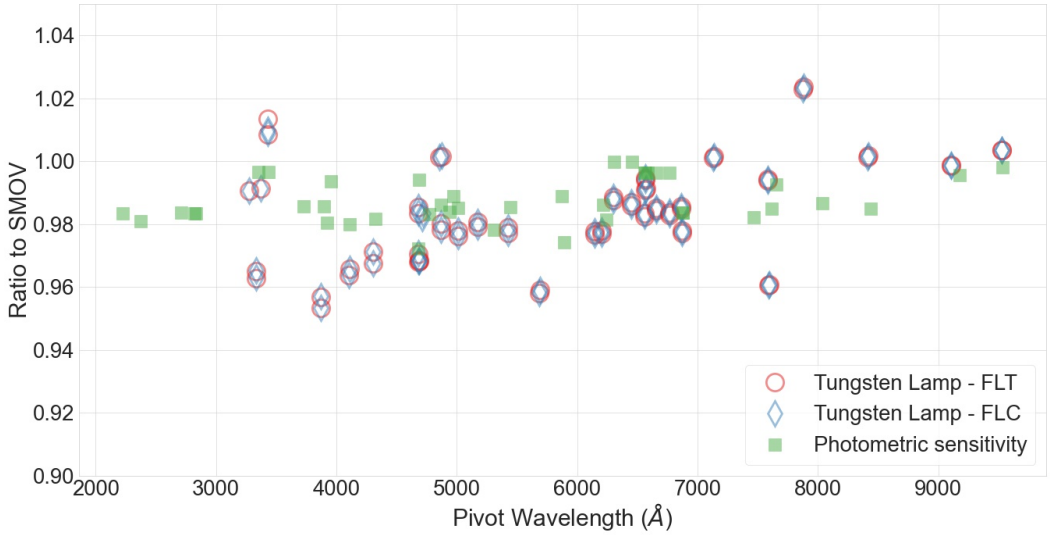

Figure 1: Ratio of tungsten internal flat-field images (2021-to-SMOV) versus pivot wavelength (in angstroms) of the filter shown in orange circles. Photometric sensitivity losses from 2009 to 2021 per Calamida et al. (2021) are shown in green squares. FLT data are open red circles, and FLC data are represented by blue diamonds.

4 Conclusions

Flux levels in UVIS flat-field images taken with tungsten lamp 3 from 2009 (SMOV) to 2021 show an overall decrease in countrates from 1-4% depending on wavelength. Some of the

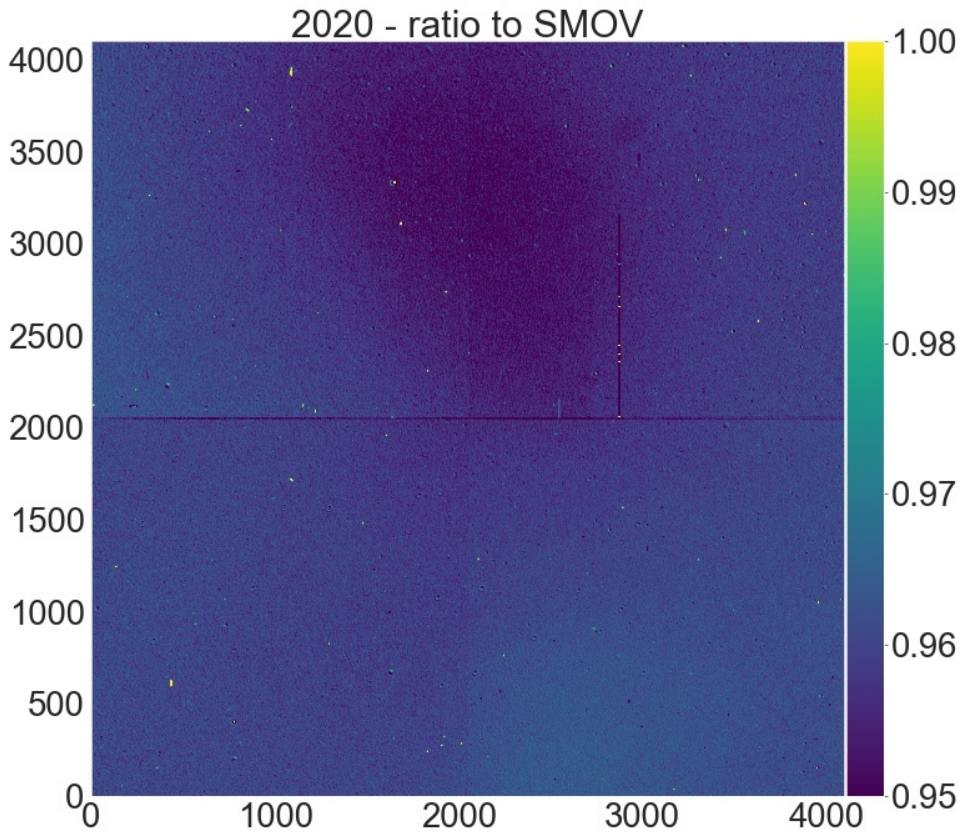

Figure 2: Ratio of tungsten internal flat-field images (2020-to-SMOV FLT) for F390W, with colorbar representing a range between 0.95 to unity. The dark patch on the top half of the image (dubbed the Bowling Pin) between the left and right quadrants (amps A and B) is clearly visible. The Roller shade is partially visible as well from (2048, 2048) to (2700, 3000). The partial dark line segment is a bad column.

decrease in brightness is associated with the known photometric sensitivity losses (Calamida et al. (2021)). Bluer wide-band filters show greater loss in performance (beyond the known photometric sensitivity decline), compared to redder filters. The cause is unknown but would be consistent with a reddening of the lamp output perhaps due to cooling of the filament and/or contamination on an optic within the calibration subsystem. New artifacts in internal tungsten flatfield ratio images have been described, most notably a dark patchy region, dubbed the Bowling Pin, in amps A and B in filters F390W, F410M, F438W, F467M, F469N, and F475W. We have not yet determined the cause of the bowling pin artifact. There is also a rectangular dark region, dubbed the Roller Shade, on filters F390W, F438W, F657N, and F658N in amp B, whose right edge coincides with one of the lithographic lines on the chip. These regions show a decrease in brightness larger than the median value of the filter ratio and typically on the order of <1 to 3% for the roller shade and 2-5% for the bowling

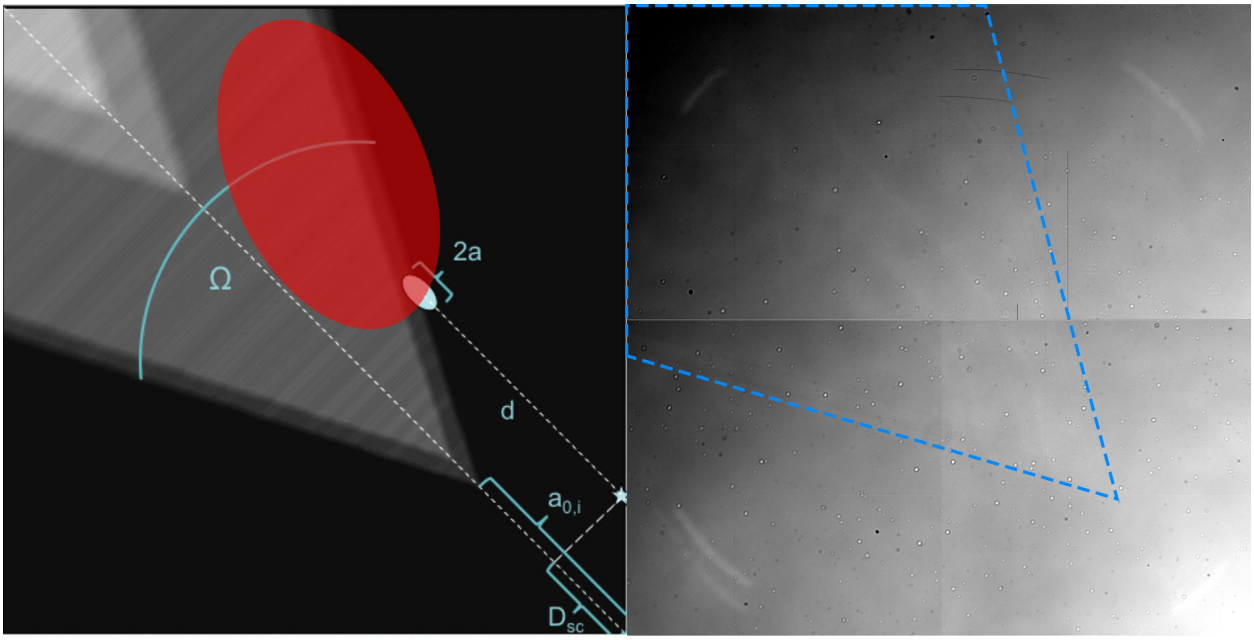

Figure 3: Left: UVIS flare effect overlayed with an approximate oval shape representing the Bowling Pin. Flare image taken from Figure 3 in McCullough (2011). Right: Example F763M UVIS tungsten flat-field image from program 11422 (iaa302j4q) with the flare visible.

pin. No new dust motes or droplets are visible in data taken since SMOV in 2009 and the existing particulates have shown that the filter wheel is not always precise in returning to its nominal position.

5 Acknowledgments

We'd like to thank Sylvia Baggett, Jennifer Mack, Peter McCullough for their invaluable insight, input, and discussions. We'd also like to thank Catherine Martlin, Joel Green, and Frederick Dauphin for their extensive review of this report. We'd like to specially thank Christopher Robert Penn from San Diego, CA for coining the name of "Bowling Pin" for the dark patchy region between amps A and B - En Taro Tassadar.

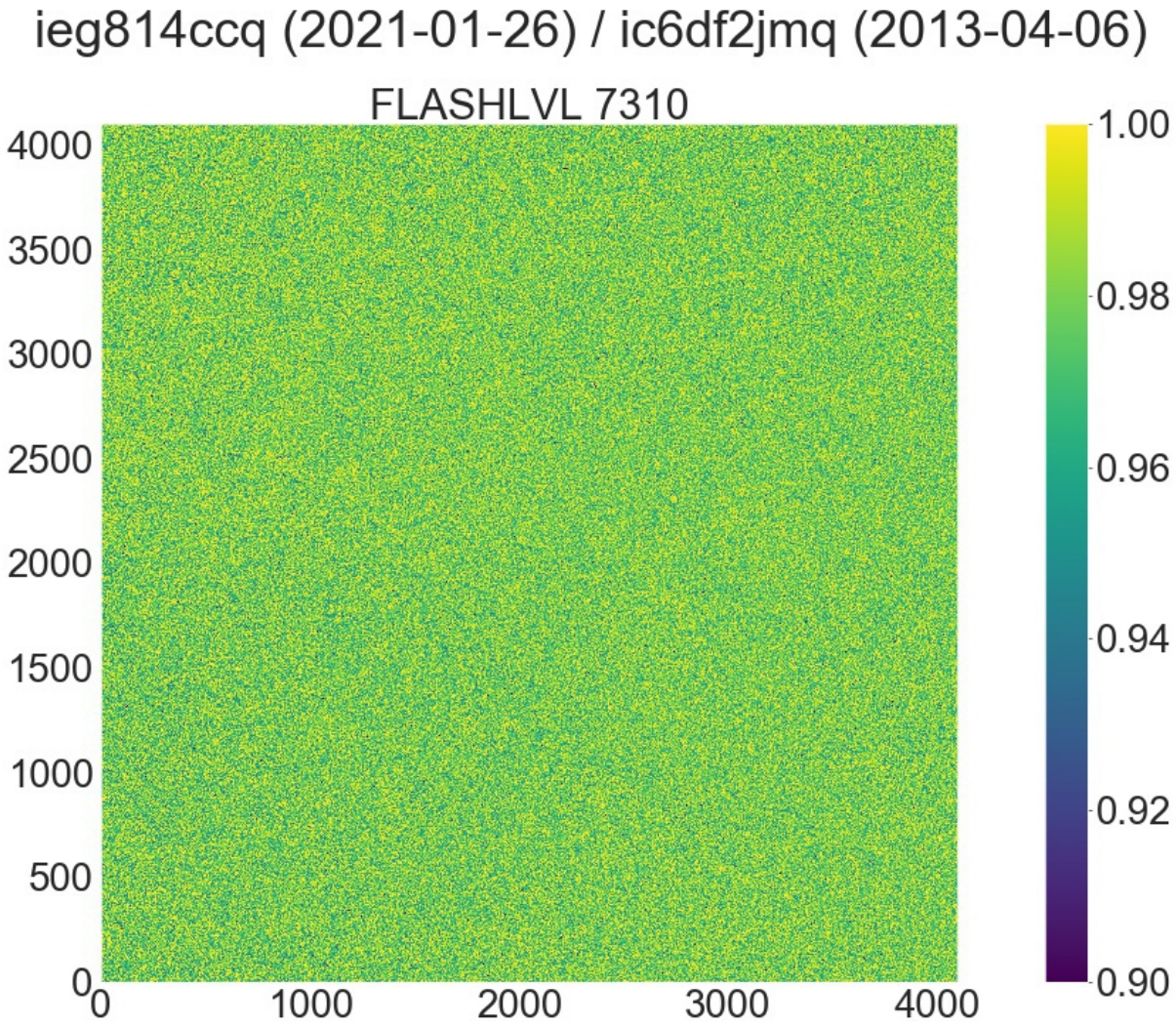

Figure 4: Ratio of a post-flashed dark image obtained in 2021 to a post-flashed dark image obtained in 2013 when post-flashing became available for use. Both images received a post-flash stimulus of 7310 electrons per pixel.

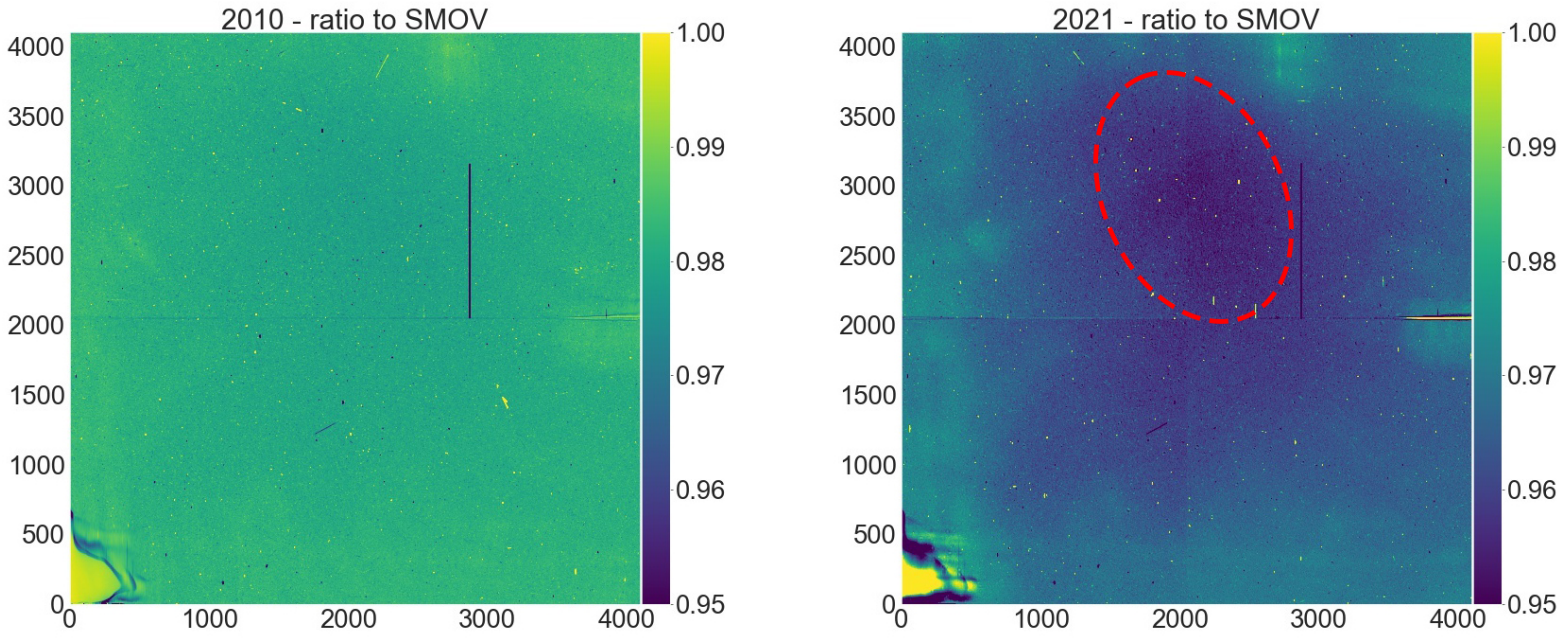

Figure 5: Ratio of tungsten internal flat-field images for F410M, with colorbar representing a range between 0.95 to unity. **Left**: Ratio is 2010-to-SMOV FLT, several unique features are present, including the structure in the lower left amp C quadrant and others along the perimeter of the image ratio. **Right**: Ratio is 2021-to-SMOV FLT, note the presence of the dark patch between amps A & B (the Bowling Pin) outlined in red.

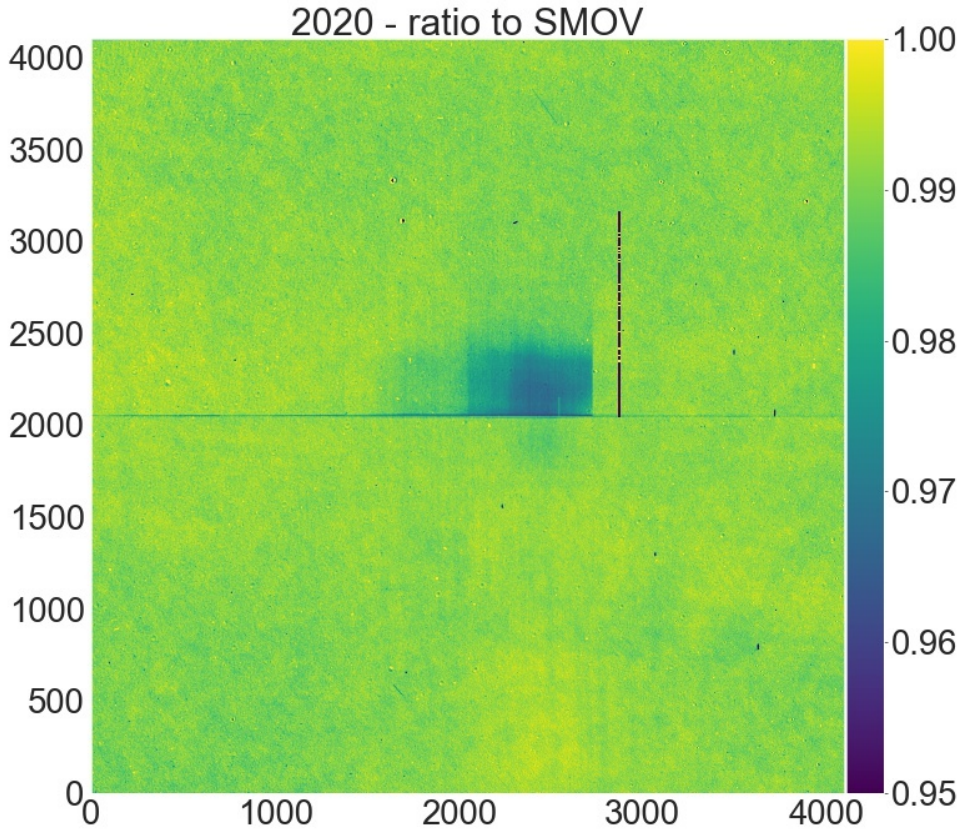

Figure 6: Ratio of tungsten internal flat-field images (2020-to-SMOV FLT) for F658N, with colorbar representing a range between 0.95 to unity. A streak is visible in Amp B above the chip gap we have dubbed the roller shade. The right edge of the feature coincides with the edge of one of the photolithographic sections of the chip.

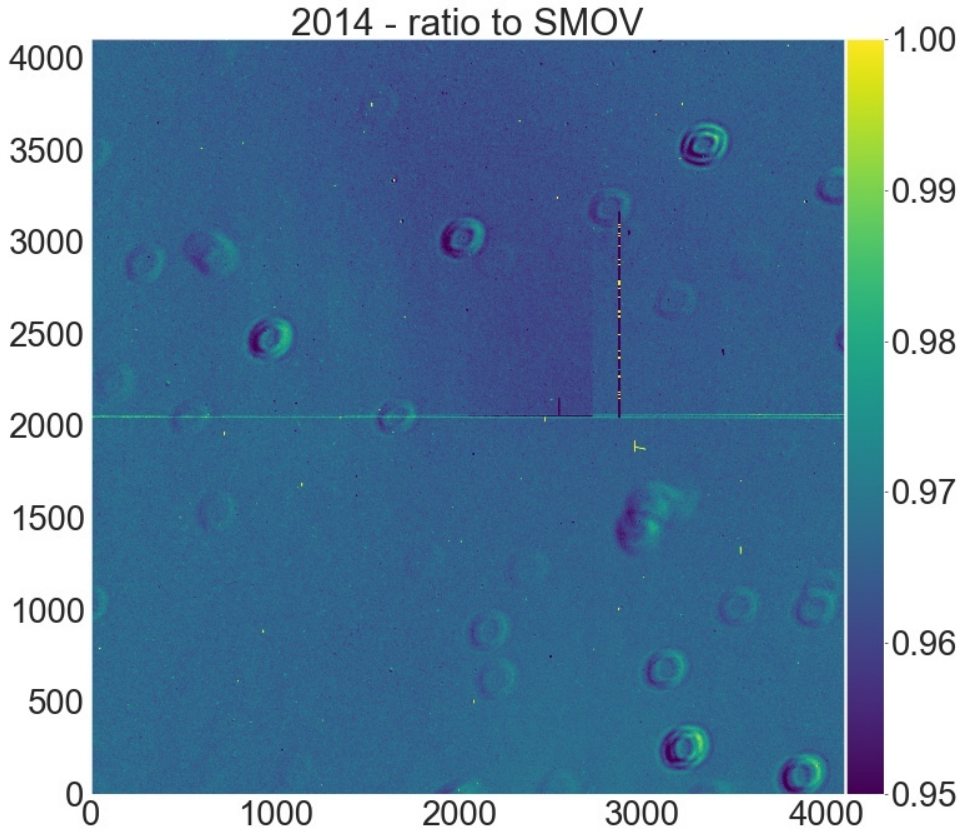

Figure 7: Ratio of tungsten internal flat-field images (2014-to-SMOV FLT) for F438W, with colorbar representing a range between 0.95 to unity. The roller shade is visible in amp B. Other artifacts such as droplets and dust motes can also be seen across the detector.

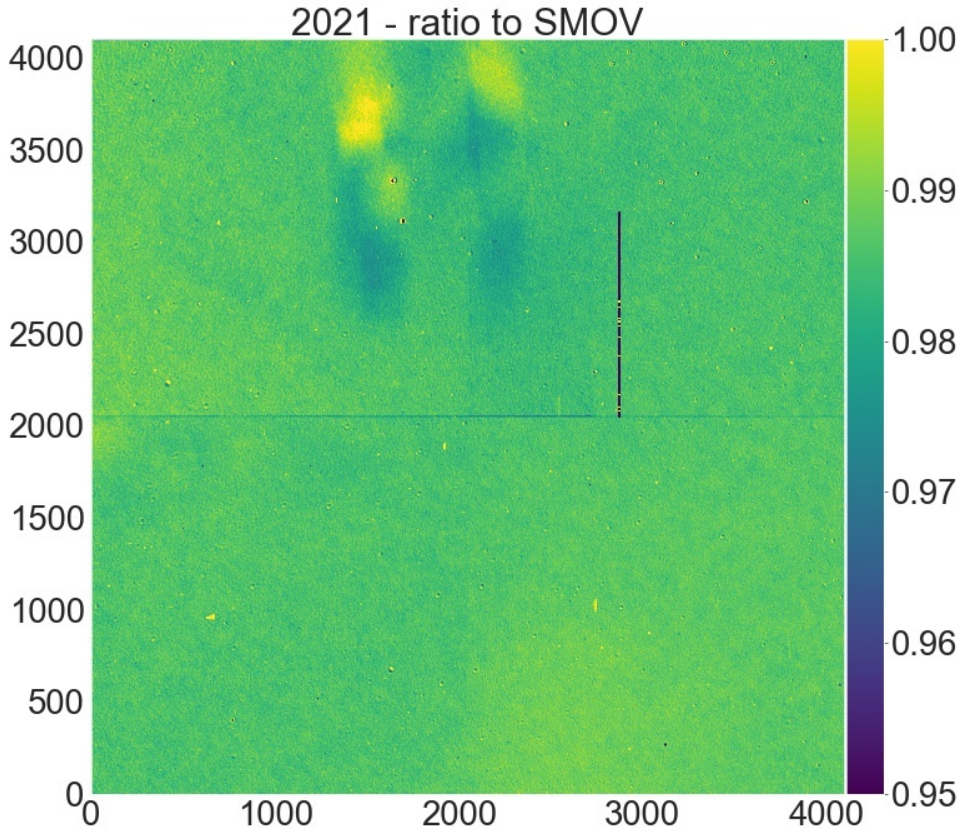

Figure 8: Ratio of tungsten internal flat-field images (2021-to-SMOV FLT) for F645N, with colorbar representing a range between 0.95 to unity. An H-shaped pattern, present since launch (Baggett, Sabbi, and McCullough (2009)), is visible encompassing amps A and B.

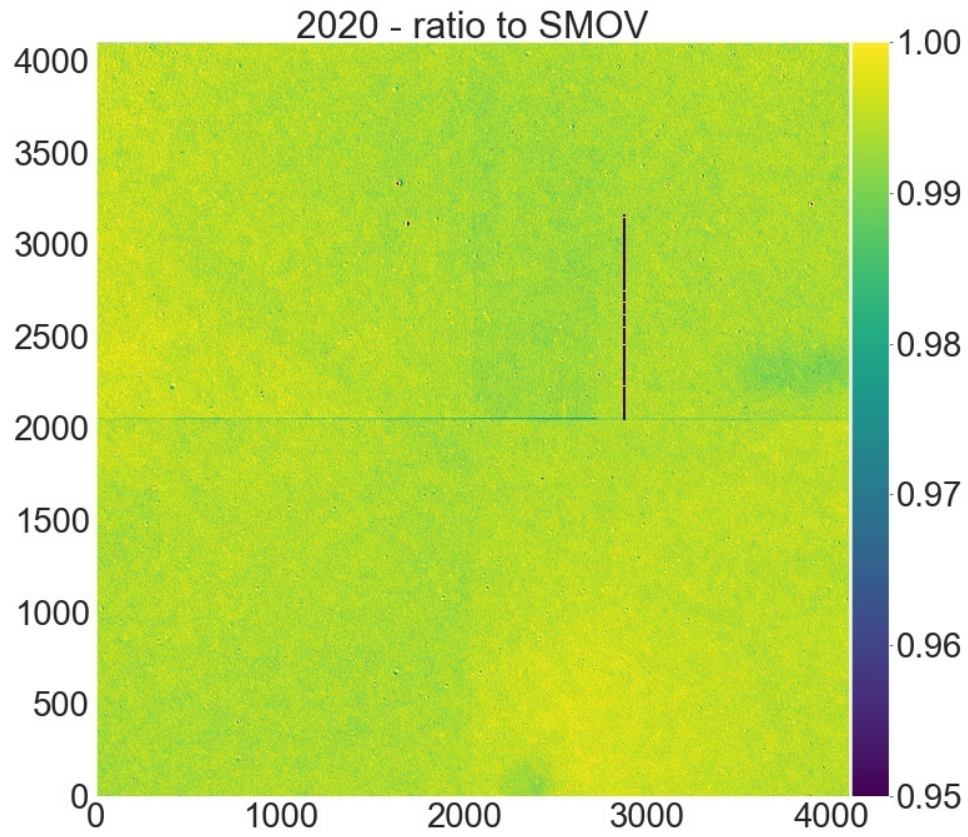

Figure 9: Ratio of tungsten internal flat-field images (2020-to-SMOV FLT) for F657N, with colorbar representing a range between 0.95 to unity. Dark regions on the lower right of amp B, and on amp D can be seen, and some of the roller shade is also visible. The partial dark line is a bad column.

References

Baggett, S. (Oct. 2008). *WFC3 TV3 Testing: UVIS Channel Calibration Subsystem Performance*. Space Telescope WFC Instrument Science Report.

Baggett, S., E. Sabbi, and P. McCullough (Nov. 2009). *WFC3 SMOV Proposal 11422/11529: UVIS SOFA and Lamp Checks*. Space Telescope WFC Instrument Science Report.

Bourque, M. and S. Baggett (June 2013). *WFC3/UVIS Bowtie Monitor*. Space Telescope WFC Instrument Science Report.

Calamida, Annalisa et al. (Feb. 2021). *New time-dependent WFC3 UVIS inverse sensitivities*. Space Telescope WFC Instrument Science Report.

Gunning, H., S. Baggett, and J. MacKenty (Sept. 2014). *Pixel-to-Pixel Flat field Changes in WFC3/UVIS*. Space Telescope WFC Instrument Science Report.

Kozhurina-Platais, V. et al. (July 2013). *Astrometric Correction for WFC3/UVIS Lithographic-Mask Pattern*. Space Telescope WFC Instrument Science Report.

Mack, J., E. Sabbi, and T. Dahlen (June 2013). *In-flight Corrections to the WFC3 UVIS Flat Fields*. Space Telescope WFC Instrument Science Report.

McCullough, P. (Jan. 2011). *Geometric model of UVIS window ghosts in WFC3*. Space Telescope WFC Instrument Science Report.

Rajan, A. and S. Baggett (Jan. 2010). *WFC3 SMOV Proposal 11432: UVIS Internal Flats*. Space Telescope WFC Instrument Science Report.

Table 1: WFC3/UVIS tungsten lamp flat data used (1 of 2)

Filter	**Program IDs (date range)**	**# of images**
F200LP	11422, 11432, 11529, 12711, 13097, 13586, 14028, 14390, 14547, 14997, 15590, 15730, 16410 (**2009.44 - 2021.16**)	16
F336W	11426, 11907 (**2009.48 - 2010.77**)	44
F343N	12693 (**2011.83 - 2011.84**)	17
F350LP	11422, 11432, 11454, 11529, 11912, 12711, 13097, 13586, 14028, 14390, 14547, 14997, 15590, 15730, 16410 (**2009.41 - 2021.16**)	34
F390M	12347 (**2010.83 - 2010.92**)	4
F390W	11432, 12337, 12347, 12711, 13097, 13586, 14028, 14390, 14547, 14997, 15590, 15730, 16410 (**2009.50 - 2020.96**)	38
F410M	11432, 11912, 12711, 13097, 13586, 14028, 14390, 14547, 14997, 15590, 15730, 16410 (**2009.50 - 2021.17**)	19
F438W	11426, 11432, 11912, 12337, 12343, 12347, 12711, 12808, 13097, 13169, 13585, 13586, 14027, 14028, 14389, 14390, 14546, 14547, 14996, 14997, 15589, 15590, 15729, 15730, 16409, 16410 (**2009.48 - 2021.16**)	1116
F467M	11422, 11432, 11529, 11912, 11925, 12337, 12693, 12711, 13097, 13586, 14027, 14028, 14390, 14547, 14997, 15590, 15730, 16410 (**2009.44 - 2021.16**)	82
F469N	11432, 11912, 12693, 12711, 13097, 13586, 14028, 14390, 14547, 14997, 15590, 15730, 16410 (**2009.50 - 2021.16**)	33
F475W	11432, 11912, 12711, 13097, 13586, 14028, 14390, 14547, 14997, 15590, 15730 (**2009.50 - 2020.17**)	30
F475X	11422, 11432, 11529, 11808, 11908, 11909, 11912, 12343, 12344, 12687, 12688, 12711, 13071, 13072, 13097, 13103, 13104, 13554, 13555, 13586, 14000, 14001, 14028, 14366, 14367, 14390, 14529, 14530, 14547, 14978, 14979, 14997, 15567, 15568, 15590, 15712, 15713, 15730, 16393, 16410, 16414 (**2009.44 - 2021.18**)	5253
F487N	11432, 11912, 12711, 13097, 13586, 14028, 14390, 14547, 14997, 15590, 15730 (**2009.50 - 2020.17**)	18
F502N	11432, 11904, 11912, 12711, 13097, 13586, 14027, 14028, 14390, 14547, 14997, 15590, 15730 (**2009.50 - 2020.17**)	82
F547M	11432, 11912, 12711, 13097, 13586, 14027, 14028, 14390, 14547, 14997, 15590, 15730, 16410 (**2009.50 - 2021.18**)	74
F555W	11422, 11432, 11529, 11904, 11912, 12337, 12711, 13097, 13586, 14028, 14390, 14547, 14997, 15590, 15730, 16410 (**2009.44 - 2021.17**)	45
F600LP	11432, 11912, 12711, 13097, 13586, 14028, 14390, 14547, 14997, 15590, 15730, 16410 (**2009.50 - 2021.16**)	31
F606W	11422, 11426, 11432, 11454, 11529, 11907, 11912, 12337, 12711, 13097, 13586, 14028, 14390, 14547, 14997, 15590, 15730, 16410 (**2009.41 - 2020.96**)	105
F621M	11432, 11912, 12711, 13097, 13586, 14027, 14028, 14390, 14547, 14997, 15590, 15730, 16410 (**2009.50 - 2021.17**)	64
F625W	11422, 11432, 11529, 11912, 12711, 13097, 13586, 14028, 14390, 14547, 14997, 15590, 15730, 16410 (**2009.44 - 2021.17**)	23
F631N	11432, 11912, 12711, 13097, 13586, 14028, 14390, 14547, 14997, 15590, 15730 (**2009.50 - 2020.17**)	24

Table 2: WFC3/UVIS tungsten lamp flat data used (2 of 2)

Filter	**Program IDs (date range)**	**# of images**
F645N	11422, 11432, 11529, 11912, 12711, 13097, 13586, 14028, 14390, 14547, 14997, 15590, 15730, 16410 (**2009.44 - 2021.18**)	21
F656N	11422, 11432, 11529, 11912, 12337, 12711, 13097, 13586, 14028, 14390, 14547, 14997, 15590, 15730, 16410 (**2009.44 - 2021.18**)	32
F657N	11422, 11432, 11529, 11912, 12711, 13097, 13586, 14028, 14390, 14547, 14997, 15590, 15730 (**2009.44 - 2020.17**)	20
F658N	11432, 11912, 12711, 13097, 13586, 14028, 14390, 14547, 14997, 15590, 15730 (**2009.50 - 2020.17**)	24
F665N	11432, 11912, 12711, 13097, 13586, 14028, 14390, 14547, 14997, 15590, 15730, 16410 (**2009.50 - 2021.17**)	25
F673N	11432, 11912, 12711, 13097, 13586, 14028, 14390, 14547, 14997, 15590, 15730, 16410 (**2009.50 - 2021.17**)	25
F680N	11432, 11912, 12711, 13097, 13586, 14028, 14390, 14547, 14997, 15590, 15730, 16410 (**2009.50 - 2021.18**)	19
F689M	11432, 11912, 12711, 13097, 13586, 14028, 14390, 14547, 14997, 15590, 15730, 16410 (**2009.50 - 2021.17**)	19
F763M	11422, 11432, 11529, 11912, 12711, 13097, 13586, 14028, 14390, 14547, 14997, 15590, 15730, 16410 (**2009.44 - 2021.16**)	21
F775W	11432, 11912, 12337, 12711, 13097, 13586, 14028, 14390, 14547, 14997, 15590, 15730, 16410 (**2009.50 - 2021.17**)	30
F814W	11432, 11904, 11912, 12337, 12343, 12711, 12808, 13097, 13169, 13585, 13586, 14027, 14028, 14389, 14390, 14546, 14547, 14996, 14997, 15589, 15590, 15729, 15730, 16409, 16410 (**2009.50 - 2021.16**)	1103
F845M	11432, 11912, 12711, 13097, 13586, 14028, 14390, 14547, 14997, 15590, 15730, 16410 (**2009.50 - 2021.17**)	19
F850LP	11432, 11912, 12711, 13097, 13586, 14028, 14390, 14547, 14997, 15590, 15730, 16410 (**2009.50 - 2021.17**)	21
F953N	11432, 11912, 12711, 13097, 13586, 14028, 14390, 14547, 14997, 15590, 15730, 16410 (**2009.50 - 2021.16**)	19

Table 3: WFC3/UVIS tungsten lamp flat ratio of the most recent data (2020/2021 unless noted) to SMOV (2009)

Filter	Average Pivot Wavelength (Å)	Ratio to SMOV Chip 1	Ratio to SMOV Chip 2
F200LP	3323.1	0.99	0.99
F336W	3336.0	0.96	0.96
F343N	3429.7	1.00	1.01
F350LP	4866.8	1.00	1.00
F390W	3870.8	0.95	0.95
F410M	4107.5	0.96	0.96
F438W	4307.4	0.97	0.96
F467M	4679.4	0.97	0.96
F469N	4687.8	0.96	0.96
F475W	4680.2	0.98	0.98
F487N	4871.8	0.98	0.97
F502N	5009.2	0.97	0.97
F547M	5425.1	0.97	0.97
F555W	5172.4	0.98	0.97
F600LP	7132.7	1.00	1.00
F606W	5688.3	0.95	0.95
F621M	6201.7	0.97	0.97
F625W	6147.5	0.97	0.97
F631N	6303.3	0.98	0.98
F645N	6452.5	0.98	0.98
F656N	6560.0	0.98	0.98
F657N	6565.9	0.99	0.99
F658N	6569.4	0.99	0.99
F665N	6655.9	0.98	0.98
F673N	6765.1	0.98	0.98
F680N	6872.4	0.97	0.97
F689M	6863.2	0.98	0.98
F763M	7593.4	0.96	0.96
F775W	7584.0	0.99	0.99
F814W	7878.3	1.02	1.02
F845M	8415.1	1.00	1.00
F850LP	9105.6	0.99	0.99
F953N	9527.7	1.00	1.00

Table 4: Flat-field image filters with prominent features

Filter	Notes
F390W	Bowling Pin visible from 2010 onwards, darkening over time. Lithography area (roller shade) also visible.
F410M	Known detector defect on left bottom corner. Bowling Pin
F438W	Bowling Pin and Roller Shade prominent. Droplets present in some years.
F467M, F469N, F475W, F487N, F502N	Bowling Pin barely visible
F645N	Known H-shaped bright region present in all years.
F657N	Known bright region in amps B and D (appear as dark regions)
F658N	Prominent Roller Shade